INTERNATIONAL JOURNAL FOR NUMERICAL METHODS IN FLUIDS
Int. J. Numer. Meth. Fluids 2006; **50**:751–764
Published online 15 September 2005 in Wiley InterScience (www.interscience.wiley.com). DOI: 10.1002/fld.1078

Non-Newtonian blood flow dynamics in a right internal carotid artery with a saccular aneurysm

Alvaro Valencia[1,*,†], Alvaro Zarate[1], Marcelo Galvez[2] and Lautaro Badilla[2]

[1]*Department of Mechanical Engineering, Universidad de Chile, Santiago, Chile*
[2]*Instituto de Neurocirugia Dr. Asenjo, Santiago, Chile*

SUMMARY

Flow dynamics plays an important role in the pathogenesis and treatment of cerebral aneurysms. The temporal and spatial variations of wall shear stress in the aneurysm are hypothesized to be correlated with its growth and rupture. In addition, the assessment of the velocity field in the aneurysm dome and neck is important for the correct placement of endovascular coils. This work describes the flow dynamics in a patient-specific model of carotid artery with a saccular aneurysm under Newtonian and non-Newtonian fluid assumptions. The model was obtained from three-dimensional rotational angiography image data and blood flow dynamics was studied under physiologically representative waveform of inflow. The three-dimensional continuity and momentum equations for incompressible and unsteady laminar flow were solved with a commercial software using non-structured fine grid with 283 115 tetrahedral elements. The intra-aneurysmal flow shows complex vortex structure that change during one pulsatile cycle. The effect of the non-Newtonian properties of blood on the wall shear stress was important only in the arterial regions with high velocity gradients, on the aneurysmal wall the predictions with the Newtonian and non-Newtonian blood models were similar. Copyright © 2005 John Wiley & Sons, Ltd.

KEY WORDS: *in vivo*; cerebral aneurysm; 3D rotational angiography; non-Newtonian fluid; computational fluid dynamics

INTRODUCTION

Cerebral aneurysms are pathological dilations of an artery, generally found in and about the circle of Willis. Cerebral aneurysms involve both the anterior circulation and the posterior circulation. Anterior circulation aneurysms arise from the internal carotid artery or any of

*Correspondence to: Alvaro Valencia, Department of Mechanical Engineering, Universidad de Chile, Casilla 2777, Santiago, Chile.
†E-mail: alvalenc@ing.uchile.cl

Contract/grant sponsor: FONDECYT Chile; contract/grant number: 1030679

Received 28 March 2005
Revised 8 July 2005
Accepted 17 July 2005

its branches, whereas posterior circulation aneurysms arise from the vertebral artery, basilar artery, or any of their branches. Rupture of an intracranial saccular aneurysm generally causes subarachnoid haemorrhage (SAH) with severe neurological complications [1].

Intracranial aneurysms are classified into saccular and non-saccular types according to their shape and etiology. Non-saccular aneurysms include atherosclerotic, fusiform, traumatic, and mycotic types. Saccular aneurysms have several anatomic characteristics that distinguish them from other types of intracranial aneurysms. Typically, saccular aneurysms arise at a bifurcation or along a curve of the parent vessel [1]. Classical treatments of saccular aneurysms are direct surgical clipping or endovascular coil insertion. Aneurysm coiling consists on the placement of coils inside the aneurysm using micro catheters introduced through the femoral artery. The coils promote blood coagulation inside the aneurysm avoiding blood flow [1].

Several theories attempt to explain the origin of intracranial aneurysms. A defect in the internal elastic lamina of arterial walls was initially postulated as the responsible mechanism in the genesis of saccular aneurysms. However, numerous histologic and experimental studies have failed to reveal evidence that supports this theory. Currently, the most important pathogenetic factor in aneurysmal formation is considered to be an area of wall degeneration in regions of haemodynamic stress. For this reason, haemodynamic studies on models of saccular aneurysms are very important in order to obtain quantitative values of the haemodynamic stress [2].

The aneurysm wall is composed of layered collagen. Wall strength is related to both collagen fibre strength and orientation. The main characteristic of the aneurysm wall is its multidirectional collagen fibres; with physiological pressures they become straight and thereby govern the overall stiffness of the lesion [3]. Wall shear stress modulates endothelial cell remodelling via realignment and elongation, and the time variation of wall shear stress affects significantly the rates at which endothelial cells remodel [4].

Although aneurysm rupture is thought to be associated with a significant change in aneurysm size, there is still great controversy regarding the size at which rupture occurs. Rupture occurs preferentially at the site of the dome, particularly in daughter aneurysms. The relationship between geometric features and rupture is closely associated with low flow conditions [5].

Liou and Liou [6] presented a review of *in vitro* studies of haemodynamic characteristics in terminal and lateral aneurysm models. They reported in terminal aneurysms that for uneven branch flow, the flow activity inside the aneurysm and the shear stresses acting on the intra-aneurysmal wall increase with increasing bifurcation angle. Imbesi and Kerber [7] have used *in vitro* models to study the flow into a wide-necked basilar artery aneurysm. They investigated the flow after placement of a stent across the aneurysm neck and after placement of Guglielmi detachable coils inside the aneurysm sac through the stent. Lieber *et al*. [8] have studied, using particle image velocimetry, the influence of stent design on intra-aneurysmal flow in a model of a lateral saccular aneurysm. Their results show that stents can induce favourable changes in the intra-aneurysmal haemodynamics.

Arterial compliance contributes to the final determination of the mechanical conditions and outcome of the vessel [9]. This effect has not been considered in the reported studies of haemodynamics in cerebral arteries with aneurysms. The influence of non-Newtonian properties of blood on the arterial flow was investigated by Gijsen *et al*. [10]. They performed laser Doppler anemometry experiments and finite element simulations of steady flow in a three-dimensional model of the carotid bifurcation. A comparison between the experimental

and numerical results showed good agreement, for both Newtonian and non-Newtonian fluids. Johnston *et al.* [11] compare the influence of different non-Newtonian models on wall shear stress in coronary arteries. It is concluded that, it is advisable to use power law models in order to achieve better approximation of wall shear stress on regions with low shear stress. The influence of non-Newtonian properties of blood in an idealized arterial bifurcation model with a saccular aneurysm has been investigated in Reference [12], in the regions with relatively low velocities there is no essential difference in the results with both fluid models.

Tateshima *et al.* [13] studied the intra-aneurysmal flow dynamics in acrylic models obtained using three-dimensional computerized tomography angiography. They showed that the flow velocity structures were dynamically altered throughout the cardiac cycle, particularly at the aneurysm neck. Ma *et al.* [14] have recently performed a three-dimensional geometrical characterization of cerebral aneurysms from computed tomography angiography data, reconstructing the geometry of unruptured human cerebral aneurysms. This geometry can be classified as hemisphere, ellipsoid, or sphere.

Steinman *et al.* [15] reported image-based computational simulations of the flow dynamics for Newtonian fluid in a giant anatomically realistic human intracranial aneurysm. Computational fluid dynamics analysis revealed high-speed flow entering the aneurysm at the proximal and distal ends of the neck, promoting the formation of both persistent and transient vortices within the aneurysm sac. This produced dynamic patterns of elevated and oscillatory wall shear stresses distal to the neck and along the sidewalls of the aneurysm. The pulsatile flow in a cerebral arterial segment exhibiting two saccular aneurysms was investigated in Reference [16], they show that the two aneurysms behave in a dissimilar manner, since the blood inflow region oscillates only in one of them. This information can help to design the optimal intervention, particularly in cases where the obliteration of the aneurysm is difficult.

Cebral *et al.* [17] performed computational analysis of blood flow dynamics in cerebral aneurysms from computed tomography angiography and 3D rotational angiography image data. They discussed the limitations and difficulties of *in vivo* image-based CFD. The image data obtained with 3D rotational angiography with more than one feeding vessel may be incomplete, the specification of the correct physiologic flow conditions for each individual patient is also a limitation and other important assumption is that of rigid vessel walls. Despite these limitations, the methodology can be used to study possible correlations between intra-aneurysmal flow patterns and the morphology of the aneurysm and eventually the risk of rupture. Cebral *et al.* [18] presented a sensitivity analysis of the haemodynamic characteristics with respect to variations of several variables in patient-specific models of cerebral aneurysms, they found that the variable that has the greater effect on flow field is the geometry of the vessel.

In this work, we present detailed numerical simulations of three-dimensional unsteady flow in a model of internal carotid artery with a saccular aneurysm constructed from 3D rotational angiography image data. The purpose of this study is to report the effects of non-Newtonian blood properties on flow characteristics and wall shear stress. This investigation provides valuable insight in the study of saccular aneurysms subject to physiologically realistic pulsatile loads. In addition, pre-procedural planning for cerebral aneurysm endovascular treatments will benefit from an accurate assessment of flow patterns in the aneurysm as presented in this work by means of computational fluid dynamics techniques.

METHODS

The patient-specific model of the internal carotid artery with a saccular aneurysm is constructed from 3D rotational angiography image data. To obtain a proper anatomical representation of the model, computational fluid dynamics requires adequate reconstruction of the connected vessels. In this work the geometry is reconstructed through the union of several individual components of the internal carotid artery with saccular aneurysm. The reconstruction technique developed in this work is based on CAD techniques.

Reconstruction and grid generation

In this study, a model of the right internal carotid artery with a saccular aneurysm located adjacent to the carotid siphon was reconstructed. The images were obtained with a Philips Allura 3D rotational angiograph. The patient is a 43 year old woman without important previous neurological antecedents. For this investigation the patient gave the proper and informed consent. The 3D rotational angiography data consist in 124 images with a 0.22 mm of spacing that are obtained over 180° during intra-arterial injection of radio-opaque material. A 3D volume is reconstructed with an isotropic voxel. The volume consists in a voxel of $256 \times 256 \times 256$ pixels, see Figure 1.

The segmentation is made manually with the commercial software Freehand to obtain regular contours for each 2D image. The parametrization of the contours is made using the software 3D-Doctor. Using 3D-Doctor a three-dimensional representation of the geometry utilizing a vector-based triangularization can be obtained. The carotid syphon, the saccular aneurysm with this neck and dome, and the arterial bifurcation with the middle and anterior cerebral arteries are extracted in separate files. From different cut planes using B-spline the contours are obtained, later NURBS surfaces are generated and finally the different surfaces are pasted to create the geometry of the internal carotid artery with saccular aneurysm, see Figure 2. This geometry is exported from the CAD Software to the mesh generator Gambit

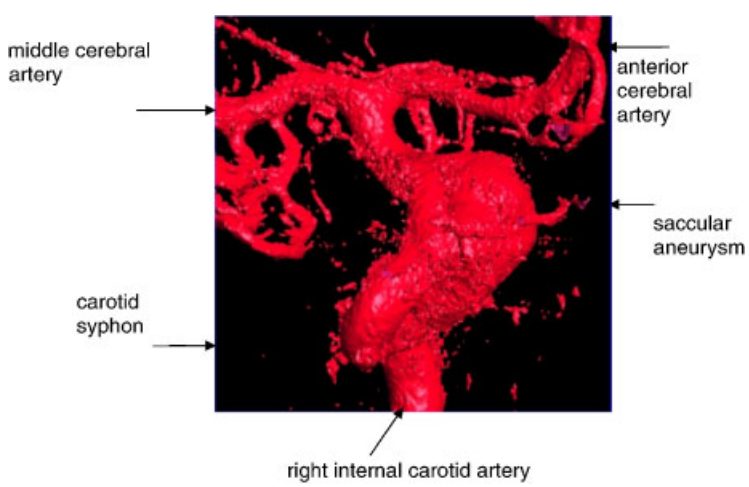

Figure 1. View of carotid artery with saccular aneurysm from 3D rotational angiography.

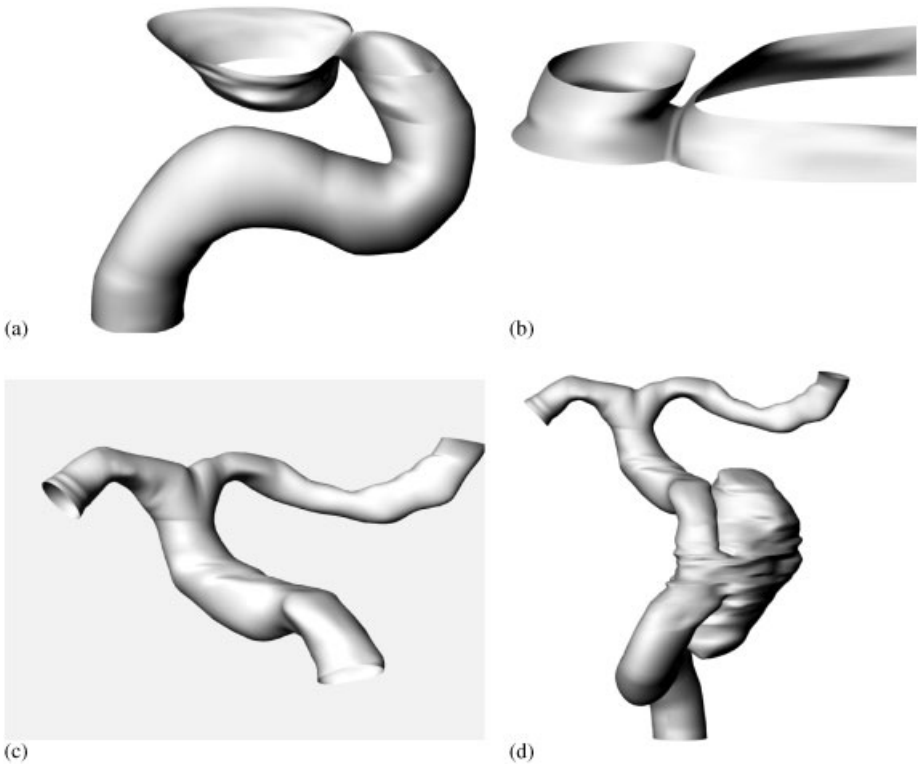

Figure 2. Reconstruction of model: (a) carotid syphon; (b) detail of union between artery and aneurysm; (c) arterial bifurcation; and (d) complete geometry of right internal carotid artery with aneurysm.

(Fluent Inc.). The created surface is regular, so that the grid size is limited only for computational capabilities. The volume enclosed by this surface is filled with tetrahedral elements using mesh options for unstructured grid implemented in Gambit.

Governing equations

The mass and momentum conservation equations for an incompressible fluid can be written as

$$\nabla \cdot \mathbf{v} = 0 \tag{1}$$

$$\rho \left(\frac{\partial \mathbf{v}}{\partial t} + \mathbf{v} \cdot \nabla \mathbf{v} \right) = -\nabla p + \nabla \cdot \boldsymbol{\tau} \tag{2}$$

where ρ is the density, $\mathbf{v}$ is the velocity field, p is the pressure, and $\boldsymbol{\tau}$ is the deviatoric stress tensor. This tensor is related with the strain rate tensor, however this relation is usually expressed as an algebraic equation of the form

$$\tau = \mu \dot{\gamma} \tag{3}$$

where μ is the viscosity and $\dot{\gamma}$ is the strain rate, which is defined for incompressible fluid as

$$\dot{\gamma} = \left(\frac{\partial v_i}{\partial x_j} + \frac{\partial v_j}{\partial x_i} \right) \tag{4}$$

For the Newtonian fluid assumption the viscosity of blood is constant, and a typical value of $\mu = 0.00319 \mathrm{Ns/m^2}$ was used. However, blood is a suspension of red blood cells in plasma. The viscosity of blood is mainly dependent on the volume fraction of red blood cells in plasma. The Herschel–Bulkley fluid model of blood assumes that the viscosity μ varies according to the law

$$\mu = k\dot{\gamma}^{n-1} + \frac{\tau_0}{\dot{\gamma}} \tag{5}$$

The Herschel–Bulkley fluid model of blood extends the simple power law model for non-Newtonian fluids to include the yield stress τ_0. Like the Casson model, it shows both yield stress and shear-thinning non-Newtonian viscosity, and it is one accurate model to describe the rheological behaviour of blood [19]. We have taken the experimental values recommended by Kim [19] as $k = 8.9721 \times 10^{-3}\ \mathrm{N\,s^n/m^2}$, $n = 0.8601$ and $\tau_0 = 0.0175\ \mathrm{N/m^2}$. The density of blood is assumed constant, $\rho = 1050\ \mathrm{kg/m^3}$, for both Newtonian and non-Newtonian fluid assumptions.

Boundary conditions

Since no flow measurement was performed in this patient, physiologically flow condition is imposed using flow measurements acquired in the same artery for a normal patient and provided by Prof. J. Cebral, George Mason University. The heart rate was 70 bpm. The mean blood flow rate in the right internal carotid artery is 289 ml/min. With $d = 3.55$ mm, we obtain a mean blood velocity in the inlet of this artery of $U = 48.7$ cm/s. The flow profile was computed with Fourier decomposition in 23 coefficients. The Womersley number, which characterizes the flow frequency, the geometry of the model and the Newtonian fluid viscous properties is $\alpha = 2.36$. Peak systolic flow occurs at $t = 0.331$ s. The boundary condition for the inlet velocity is defined by Equation (6)

$$U(t,r) = U_{\mathrm{m}}(t) \cdot \frac{3n+1}{n+1} \left[1 - \left(\frac{r}{R} \right)^{\frac{n+1}{n}} \right] \tag{6}$$

where $n = 1$ for a Newtonian fluid, $n = 0.8601$ for the Herschel–Bulkley non-Newtonian fluid model and $U_{\mathrm{m}}(t)$ is given by the flow waveform illustrated in Figure 3. For Newtonian fluid the Womersley solution should be used at inlet, however with the small $\alpha = 2.36$ the solution for $U(t,r)$ from Equation (6) is very close to the exact solution of Womersley [20]. Equation (6) is the solution of velocity profile for the Herschel–Bulkley fluid model in a tube considering $\tau_0 = 0$. The outflow boundary condition is defined by $\partial\phi/\partial n = 0$ on both cerebral arteries for all primary (ϕ) fluid variables (velocity and pressure). A no-slip condition is prescribed at the walls and a zero reference pressure ($p = 0$) is imposed at the inlet. The time-averaged Reynolds number with the Newtonian fluid assumption is $Re = 568$. The equivalent Reynolds number defined for a Herschel–Bulkley non-Newtonian fluid model with $\tau_0 = 0$ is

$$Re_{\mathrm{m}} = (\rho U^{2-n} d^n)/(8^{n-1} k (3n+1)/4n)^n) \tag{7}$$

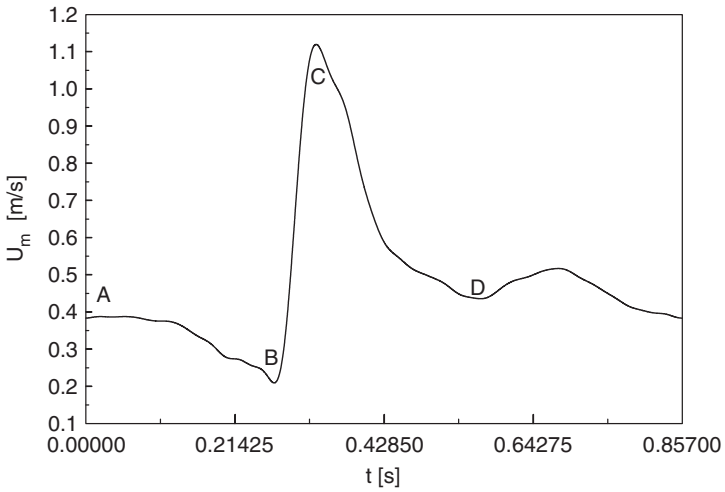

Figure 3. Physiological waveform of mean inlet velocity.

and it results $Re_{\mathrm{m}} = 521$, this value is 8% smaller as the Reynolds number for Newtonian fluid.

Numerical method

Governing Equations (1)–(5) were solved with the software FLUENT (v6.0, Fluent, Inc., Lebanon, NH), which utilizes the finite volume method for the spatial discretization. The interpolations for velocities and pressure are based on power-law and second-order, respectively. The pressure–velocity coupling is obtained using the SIMPLEC algorithm. The explicit time-marching scheme with a time step $\Delta t = 1.5 \times 10^{-5}$ s was used for the transient computations. The time step was computed from the Courant–Levy condition [21], from Equation (8). With this small time step the residual of the continuity and Navier–Stokes equations were smaller than 10^{-5} in all temporal iterations. The model of the right internal carotid artery with saccular aneurysm was meshed with 283 115 cells. The same grid size was used for the Newtonian and non-Newtonian blood assumptions. The unstructured grid was composed of tetrahedral elements

$$\Delta t = \frac{\Delta x^2}{2(\mu/\rho) + U\Delta x} \tag{8}$$

To verify grid independence, numerical simulations based on the Newtonian fluid model were performed on five grids with 64 132, 149 332, 231 782, 283 115, and 306 268 cells. The maximum pressure in the solution domain was computed in six instants of the second time period for the five grid sizes. Figure 4 shows the variation of pressure with the grid size, for the three fine grids the predictions of pressure are equal. The velocities and related stresses in the saccular aneurysm have smaller values as in the arteries, therefore the predictions in the aneurysm are even more precise. Considering that computational time increases exponentially with grid size, 283 115 cells are enough to capture the fluid dynamics in our model of the carotid artery with a saccular aneurysm. The workstation used to

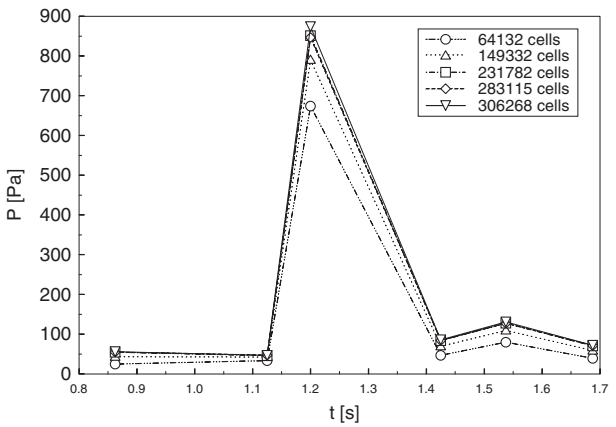

Figure 4. Variation of maximal pressure with grid size in the computational domain.

perform the simulations in this work is based on an Intel Pentium IV processor of 2.8 GHz clock speed, 1.5 GB RAM memory, and running on the Linux Redhat v8.0 operating system. The simulation time for one case based on 2 consecutive pulsatile flow cycles employing 114 286 temporal iterations was approximately 320 CPU hours. Prakash and Ethier [22] pointed out that a good quality mesh depends on many factors, including quality of the input data, robustness of the flow solver, and most importantly, the needs of the analyst. If errors around 10% are acceptable, then meshes of 200 000–250 000 cells may be sufficient for these 3D flows.

RESULTS

Flow dynamics

The non-Newtonian flow structure in the internal carotid artery with a saccular aneurysm can be seen through the pathlines at systolic time C in Figure 5. The pathlines mix as they impacted the wall of the aneurysm and then swirled as they moved to the outflow zone. The flow exits the aneurysm in a helical manner. The inflow and outflow zones in the aneurysm neck can be also observed in Figure 5 and the intra-aneurysmal flow dynamics did not show a simple pattern. The long-term anatomical durability of coil embolization of aneurysms by using existing microcoil technology depends on the aneurysm form and the blood flow dynamics in the aneurysm neck. Ideally the coil must be inserted into the inflow zone to avoid flow recanalization.

A detailed look at the flow pattern is provided in Figure 6 through velocity vectors view for the mean plane in the aneurysm and the variation over one pulsatile cycle. High velocity flow enters in the superior part of the aneurysm, travels along the aneurysm wall and enters into the core of the aneurysm. Complex vortex structures formed into the aneurysmal cavity and these change over one pulsatile cycle.

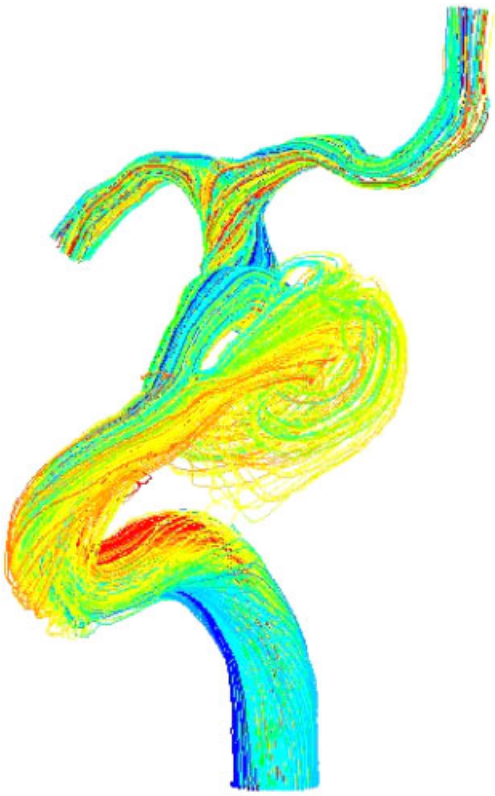

Figure 5. Instantaneous pathlines at the systolic time C.

Figure 10(a) shows the temporal dependence of velocity magnitude in the aneurysm centre with non-Newtonian and Newtonian properties of the fluid. The time variation of velocity is similar with both blood models. The velocity fields in the aneurysm with non-Newtonian and Newtonian blood model were similar, differences were found only in the internal carotid and in the cerebral arteries.

Flow-induced stresses

The pressure distribution changes on aneurysmal wall over one pulsatile cycle, as can be seen in Figure 7 for the case computed with the non-Newtonian fluid model. At systolic time C the relative pressure is around $-28\,000\,\mathrm{dyn/cm^2}$, and at the time for dicrotic notch D the pressure is around $600\,\mathrm{dyn/cm^2}$. The temporal and spatial variation of wall shear stress (WSS) on the saccular aneurysm can be observed in Figure 8. The aneurysmal dome shows the largest WSS and also the largest variation over one pulsatile cycle. At systolic time C the WSS is around $150\,\mathrm{dyn/cm^2}$ and at the time for dicrotic notch D the WSS is around $20\,\mathrm{dyn/cm^2}$. These large temporal and spatial variations of normal and tangential stresses are probably determining in the rupture of the aneurysm.

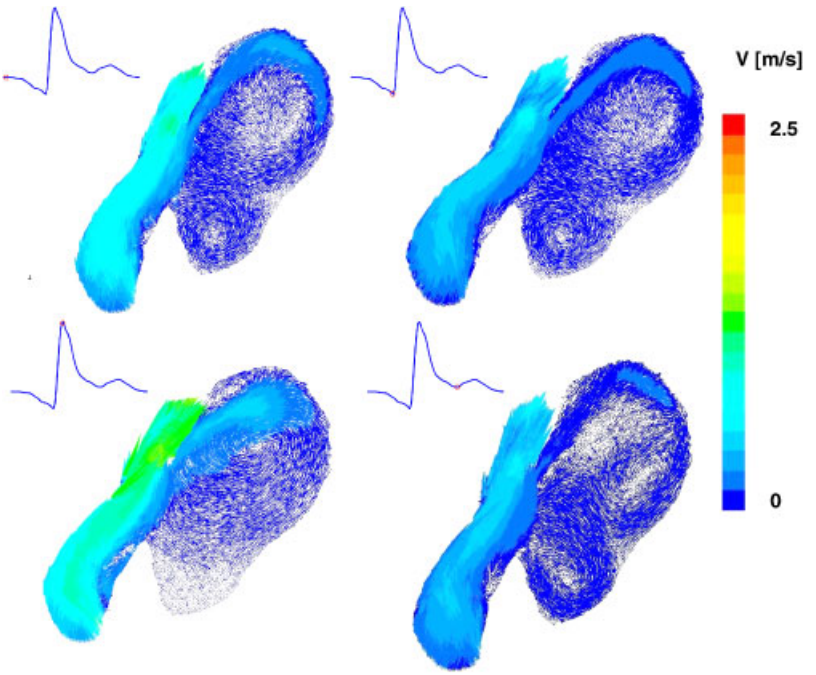

Figure 6. Velocity vectors in the aneurysmal mean plane in four instants of the pulsatile cycle.

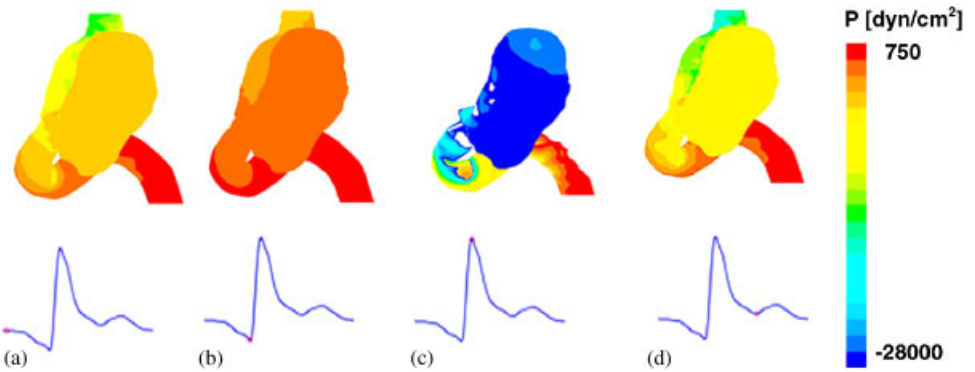

Figure 7. Contours of relative pressure on the aneurysm in four instants of the pulsatile cycle.

Figure 9 shows the WSS distribution on the right internal carotid artery with a saccular aneurysm at systolic time C computed with the non-Newtonian and Newtonian fluid models. With Newtonian fluid model the maximum of WSS is 3600 dyn/cm^2, with the non-Newtonian fluid model the maximum of WSS is only 2180 dyn/cm^2. With the Newtonian fluid model the prediction of maximum WSS is 65% higher. At the aneurysm inlet the prediction of WSS with the Newtonian fluid model can be 44% higher as with the non-Newtonian blood model.

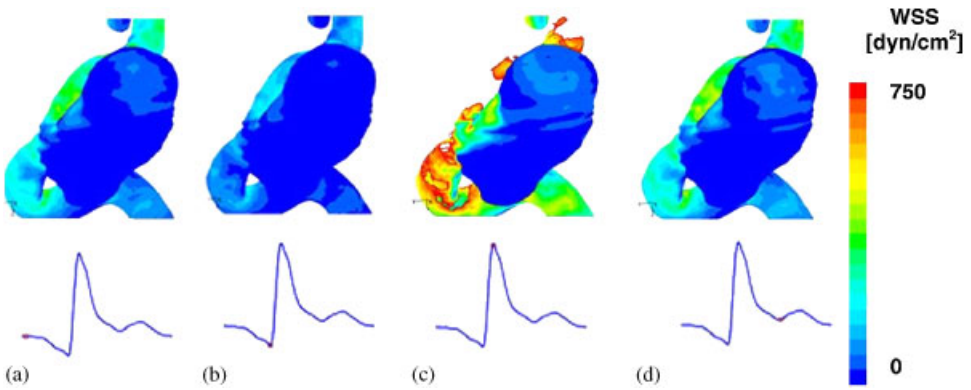

Figure 8. Contours of WSS on the aneurysm in four instants of the pulsatile cycle.

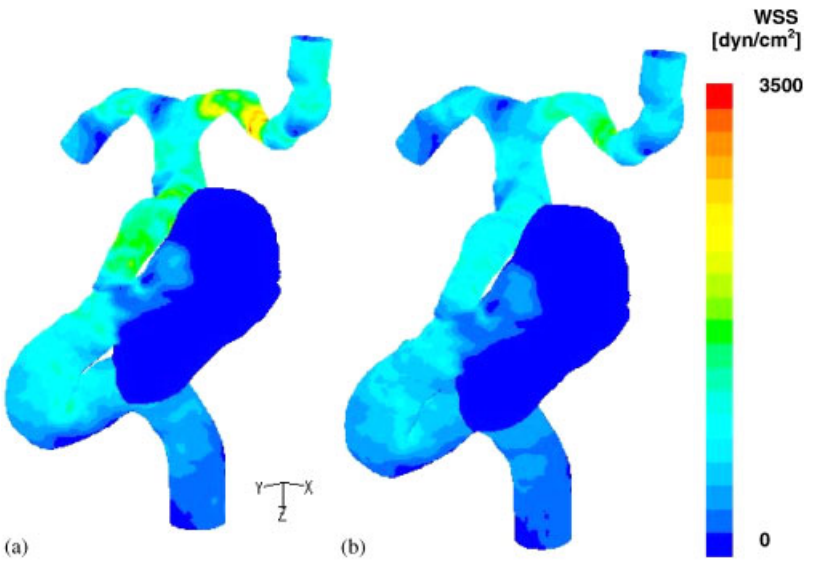

Figure 9. (a) WSS distribution at the systolic time C with Newtonian fluid model; and (b) WSS distribution at the systolic time C with non-Newtonian fluid model.

Figure 10(b) shows the time dependence of the WSS computed with non-Newtonian and Newtonian blood model at one point of the aneurysm dome, which are plotted for one pulsatile cycle. The WSS shows large variations during one pulsatile cycle. With the physiologically representative waveform of inflow, the systolic acceleration phase and the diastolic deceleration phase produce both high and low WSS on the aneurysmal wall. The temporal variations of WSS calculated with the non-Newtonian and Newtonian blood models do not show differences.

It is concluded that the predictions of velocity, pressure and WSS distributions between the Newtonian and non-Newtonian blood model differ only in regions with high velocity, particularly for the study of unsteady flow and stress distribution in a saccular aneurysm the predictions using the Newtonian blood model are reliable.

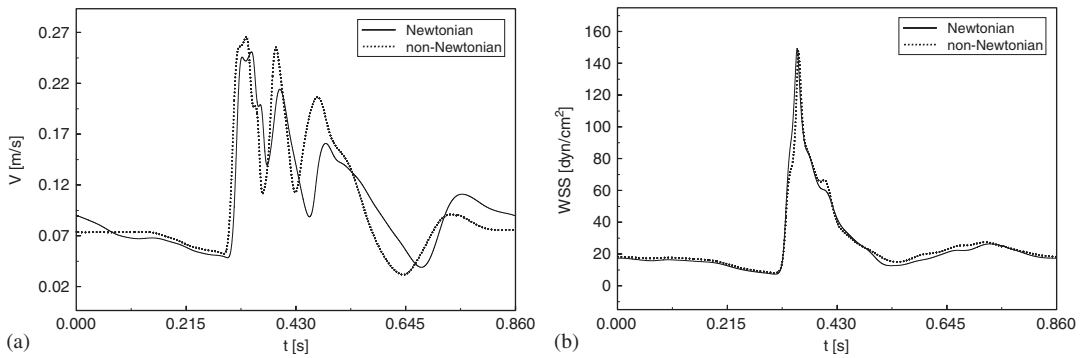

Figure 10. (a) Velocity magnitude in the aneurysm centre; and (b) WSS in one point of the aneurysm dome.

DISCUSSION

High WSS is regarded as a major factor in the development and growth of cerebral aneurysms. The endothelium is sensitive to changes in WSS and regulates local vascular tone by releasing vasodilator and vasoconstrictor substances [13]. Consequently, it has been suggested that WSS plays a major role in the adaptive dilation of arteries to a sustained increase in blood flow. The relationship between geometric features and rupture is also closely associated with very low flow conditions [23]. Localized stagnation of blood flow is known to result in the aggregation of red blood cells, as well as the accumulation and adhesion of both platelets and leukocytes along the intimal surface. This occurs due to dysfunction of flow-induced nitric oxide, which is usually released by mechanical stimulation through increased WSS. These factors may cause intimal damage, lead to small thrombus formation and infiltration of white blood cells and fibrin inside the aneurysm wall [5]. Damage to the endothelium is seen as a contributing cause to aneurysm rupture. Once the integrity of this layer of cells lining the lumen is breached, subsequent damage to the structural fibres of the vessel may occur. Blood flow is involved in the process leading to the damage of the endothelium. It is assumed that a WSS around $20\,\mathrm{dyn/cm^2}$ is suitable for maintaining the structure of the aneurysmal wall and lower WSS will degenerate endothelial cells [23]. Our results of WSS show values lower than $20\,\mathrm{dyn/cm^2}$ in large parts of the aneurysmal wall over one cardiac cycle, see Figure 8. This low WSS may be one important factor underlying the degeneration, indicating the structural fragility of the aneurysmal wall.

This numerical study of haemodynamics provides insight into the vortex dynamics and WSS originated in a patient-specific internal carotid artery with a saccular aneurysm obtained from 3D rotational angiography image data. The regions with differences on the predictions of velocity field and WSS distribution with Newtonian and non-Newtonian fluid models are shown.

Further studies are necessary to investigate the effects of arterial compliance on growth and rupture of patient-specific intracranial aneurysms. Also, the radiologic protocol for patient with aneurysms must include the patient-specific flow rate measurement with Doppler sonography. Finally numerical studies of the effects of stents and coils insertion are possible to be undertaken in patient-specific models to improve the clinical treatments.

CONCLUSIONS

This work presents a numerical investigation on the haemodynamics in a patient-specific model of the right internal carotid artery with a saccular aneurysm. The effects of Newtonian/non-Newtonian fluid modelling are studied in detail with respect to flow patterns and the spatial and temporal distributions of pressure and WSS. References are made in regards to optimal planning of endovascular coil embolization of cerebral aneurysms guided by assessment of the intra-aneurysmal flow dynamics.

The flow within the aneurysm was highly complex with transient vortex structures that change during the pulsatile cycle. The WSS shows large spatial and temporal variations on aneurysmal wall. The patient-specific analysis of the computational fluid dynamics constructed from 3D rotational angiography image data can be used to improve the outcome of aneurysm therapies.

NOMENCLATURE

a	right internal carotid artery radius
d	right internal carotid artery diameter
f	frequency
k	viscosity constant
p	pressure
Re	Reynolds number $= \rho U d/\mu$
Re_{m}	modified Reynolds number
U	mean velocity at inlet
v	velocity
WSS	wall shear stress

Greek symbols

α	Womersley number $= a(2\pi f\rho/\mu)^{1/2}$
$\dot{\gamma}$	strain rate
μ	fluid viscosity
ρ	density
τ	shear stress
τ_{w}	wall shear stress
τ_0	yield stress

ACKNOWLEDGEMENTS

The financial support received from FONDECYT Chile under Grant number 1030679 is recognized and appreciated. The authors would also like to acknowledge and thank Professor Juan Cebral, George Mason University, Fairfax, Virginia, who has kindly provided the inlet pulsatile flow of the internal carotid artery measured in a normal patient.

REFERENCES

1. Schievink WI. Intracranial aneurysms. *New England Journal of Medicine* 1997; **336**:28–40.
2. Humphrey JD, Canham PB. Structure, mechanical properties, and mechanics of intracranial saccular aneurysms. *Journal of Elasticity* 2000; **61**:49–81.
3. MacDonald DJ, Finlay HM, Canham PB. Directional wall strength in saccular brain aneurysms from polarized light microscopy. *Annals of Biomedical Engineering* 2000; **28**:533–542.
4. Hsiai TK, Cho SK, Honda HM, Hama S, Navab M, Demer LL, Ho CM. Endothelial cell dynamics under pulsating flows: significance of high versus low shear stress slew rates ($\partial\tau/\partial t$). *Annals of Biomedical Engineering* 2002; **30**:646–656.
5. Ujiie H, Tachibana H, Hiramatsu O, Hazel AL, Matsumoto T, Ogasawara Y, Nakajima H, Hori T, Takakura K, Kajiya F. Effects of size and shape (aspect ratio) on the hemodynamics of saccular aneurysms: a possible index for surgical treatment of intracranial aneurysms. *Neurosurgery* 1999; **45**:119–130.
6. Liou TM, Liou SN. A review on in vitro studies of hemodynamic characteristics in terminal and lateral aneurysm models. *Proceedings of the National Science Council ROC*(*B*) 1999; **23**:133–148.
7. Imbesi SG, Kerber CW. Analysis of slipstream flow in a wide-necked basilar artery aneurysm: evaluation of potential treatment regimens. *American Journal of Neuroradiology* 2001; **22**:721–724.
8. Lieber BB, Livescu V, Hopkins LN, Wakhloo AK. Particle image velocimetry assessment of stent design influence on intra-aneurysmal flow. *Annals of Biomedical Engineering* 2002; **30**:768–777.
9. Ho PC, Melbin J, Nesto RW. Scholarly review of geometry and compliance: biomechanical perspectives on vascular injury and healing. *ASIAO Journal* 2002; **48**:337–345.
10. Gijsen FJH, van de Vosse FN, Janssen JD. The influence of the non-Newtonian properties of blood on the flow in large arteries: steady flow in a carotid bifurcation model. *Journal of Biomechanics* 1999; **32**:601–608.
11. Johnston BM, Johnston PR, Corney S, Kilpatrick D. Non-Newtonian blood flow in human right coronary arteries: steady state simulations. *Journal of Biomechanics* 2004; **37**:709–720.
12. Perktold K, Peter R, Resch M. Pulsatile non-Newtonian blood flow simulation through a bifurcation with an aneurysm. *Biorheology* 1989; **26**:1011–1030.
13. Tateshima S, Murayama Y, Villablanca JP, Morino T, Takahashi H, Yamauchi T, Tanishita K, Viñuela F. Intraaneurysmal flow dynamics study featuring an acrylic aneurysm model manufactured using a computerized tomography angiogram as a mold. *Journal of Neurosurgery* 2001; **95**:1020–1027.
14. Ma B, Harbaugh RE, Raghavan ML. Three-dimensional geometrical characterization of cerebral aneurysms. *Annals of Biomedical Engineering* 2004; **32**:264–273.
15. Steinman DA, Milner JS, Norley CJ, Lownie SP, Holdsworth DW. Image-based computational simulation of flow dynamics in a giant intracranial aneurysm. *American Journal of Neuroradiology* 2003; **24**:559–566.
16. Chatziprodromou I, Butty V, Makhijani VB, Poulikakos D, Ventikos Y. Pulsatile blood flow in anatomically accurate vessels with multiple aneurysms: a medical intervention planning application of computational haemodynamics. *Flow*, *Turbulence and Combustion* 2003; **71**:333–346.
17. Cebral JR, Hernandez M, Frangi AF. Computational analysis of blood flow dynamics in cerebral aneurysms from CTA and 3D rotational angiography image data. *International Congress on Computational Bioengineering*, Zaragosa, Spain, 24–26 September, 2003.
18. Cebral JR, Castro MA, Appanaboyina S, Putman ChM, Millan D, Frangi AF. Efficient pipeline for image-based patient-specific analysis of cerebral aneurysm haemodynamics: technique and sensitivity. *IEEE Transactions on Medical Imaging* 2005; **24**:457–467.
19. Kim S. A study of non-Newtonian viscosity and yield stress of blood in a scanning capillary-tube rheometer. *Thesis*, Drexel University, U.S.A., 2002.
20. Zamir M. *The Physics of Pulsatile Flow*. Springer: New York, 2000.
21. Ferziger JH, Peric M. *Computational Methods for Fluid Dynamics*. Springer: Berlin, 1997.
22. Prakash S, Ross Ethier C. Requirements for mesh resolution in 3D computational haemodynamics. *Journal of Biomechanical Engineering* (ASME) 2001; **123**:134–144.
23. Shojima M, Oshima M, Takagi K, Torii R, Hayakawa M, Katada K, Morita A, Kirino T. Magnitude and role of wall shear stress on cerebral aneurysm computational fluid dynamic study of 20 middle cerebral artery aneurysms. *Stroke* 2004; **35**:2500–2505.

